Draft version September 18, 2019
Typeset using LaTeX **twocolumn** style in AASTeX61

EXTRACTING 3D GALAXY SHAPE FROM 2D IMAGE PROPERTIES USING RANDOM FORESTS

Humna Awan,[1] Alexie Leauthaud,[2] and Song Huang[2]

[1] *Department of Physics & Astronomy, Rutgers University, 136 Frelinghuysen Rd., Piscataway, NJ 08554*
[2] *Department of Astronomy and Astrophysics, University of California, Santa Cruz, 1156 High Street, Santa Cruz, CA 95064*

ABSTRACT

Galaxies are 3D objects, but we only observe their 2D projection. Extracting observational constraints on 3D galaxy shape is instrumental to aid our understanding of galaxy evolution. Here, we use a supervised machine learning algorithm to probe the relation between the 3D galaxy shape and 2D summary statistics and hence attempt to understand how much information about the 3D shape of a galaxy can be inferred from its 2D image characteristics. Specifically, we use simulated data from the Illustris and IllustrisTNG simulations, and use Random Forests to classify the 3D shape of galaxies. We find that while non-optimal, our algorithm is able to classify prolate vs. not-prolate galaxies to a certain degree; we are working on optimizing the features to improve the efficiency of our classifier. Furthermore, and perhaps more importantly, our algorithm provides a list of features that may be strong proxies for the 3D shape – the distributions of which can be compared between simulations and observations, e.g., from Hyper-Supreme Cam survey data. Also, as a by-product of our use of both Illustris and IllustrisTNG simulations, we find important differences between the two simulations: the production of lower stellar mass halos in IllustrisTNG, and comparable number of prolate vs. not-prolate galaxies in IllustrisTNG when compared to Illustris. Furthermore, we investigate the impact of using different classification criteria to classify galaxies as prolates vs. not, and find that they lead to rather different classifications – a point of caution when considering various results in literature.

Keywords: galaxy shapes, machine learning

Corresponding author: Humna Awan
awan@physics.rutgers.edu

1. INTRODUCTION

Galaxies are intrinsically 3D objects, although we lose the 3D shape information when we observe them as projected 2D objects. 3D galaxy shape is of interest to galaxy evolutionary studies, specifically for massive galaxies, e.g., since simulations reveal a connection between the prolateness of dark matter halos and their merger history (e.g., see Ceverino et al. 2015). Therefore, the ability to infer the 3D shape of galaxies from 2D summary data can help further our models for galaxy evolution while allowing testing the physicality of the simulations.

Figure 1 demonstrates the information lost between 2D projection of the 3D data and the consequent degeneracy in the 3D shape information: we see that not only there is no 1-1 correlation between the 2D effective radius, a proxy for the shape, and 3D one, the correlation depends strongly on the intrinsic 3D shape.

In order to infer the 3D shape of observed galaxies, one can take two approaches: 1) constructing 3D models for galaxies and using Bayesian inference to construct the likelihood function, and 2) using machine learning to infer the relationship between 3D shape and 2D summary statistics. While the first method is powerful, it is currently limited to work with simple toy models that do not encapsulate the variety and complexity of characteristics observed in the real data (Jiang, F. et al, in prep). In this work, we pursue the second approach, for which we utilize high resolution simulations: Illustris and IllustrisTNG. Also, aside from attempting to predict the 3D shape based on 2D summary statistics, we focus on identifying any key 2D features that may be strong proxies for the 3D shape, with the goal of eventually comparing simulations vs. observations from Hyper-Supreme Cam (HSC) survey using the distribution of these features.

We describe our method in Section 2 with results presented in Section 3, followed by a discussion and conclusion in Section 4; all our code is hosted in a `GitHub` repository[1].

2. METHODOLOGY

2.1. *Simulations and Data*

To train and test our machine learning model, we consider galaxies from Illustris-100 (Vogelsberger et al. 2014) and IllustrisTNG-100 (Nelson et al. 2018,?; Naiman et al. 2018; Springel et al. 2018; Pillepich et al. 2018a,b) simulations at $z = 0.4$ with $M_* > 10^{11} M_\odot$, leading us to 449 Illustris galaxies and 295 IllustrisTNG galaxies; the redshift is chosen to match the HSC observations. We query the server[2] to get cutout of all these galaxies, keeping track of only the stellar particles to calculate the axis ratios, as described in Section 2.3.

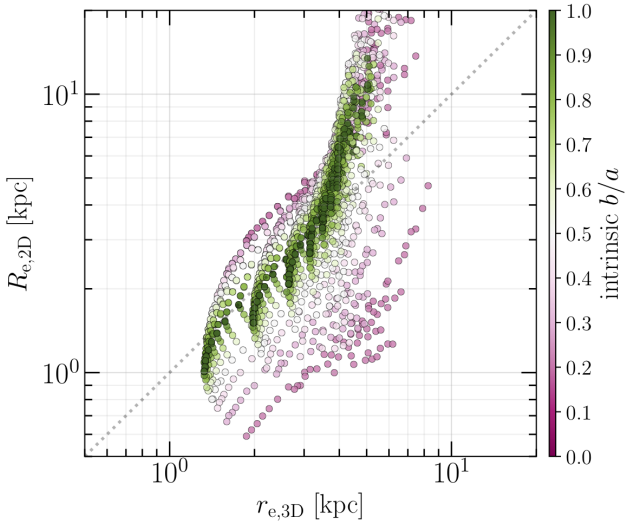

Figure 1. Figure demonstrating the degeneracy between the 2D and 3D effective radii – where effective radius of a galaxy is defined as the radius at which half of the total light of the system is emitted – a proxy for the 3D shape. Adapted from Jiang, F. et al, in prep.

As for the 2D summary data, we consider the 2D projections of the 3D galaxies from three independent viewing angles, thereby increasing our sample size by 3×. Then, using the method outlined in Huang et al. (2018), we extract summary statistics using the 1D profiles (i.e., as a function of radius) for stellar mass (M^*), ellipticity, and position angle; the method essentially fits an isophote to each galaxy to extract 1D light profiles to measure various quantities at specified radii. Furthermore, we consider second-order parameters calculated by considering the higher order moments in the Fourier expansion of the ellipse for each isophote (Kormendy et al. 2009). Specifically, we consider profiles that inform us of the "boxiness" of the isophote as well as those that encode the "asymmetry" or the effective error in the isophote-fitting process. Note, however, that these second-order parameter profiles are noisy; hence, we do not include them in the basic set of summary statistics for our training algorithm.

2.2. *Features*

For the basic set of features for our machine learning algorithm, we use the summary statistics described above. Specifically, in order to take out the dependency on the stellar mass M^*, we con-

[1] https://github.com/humnaawan/3D-galaxies-kavli

[2] http://www.tng-project.org/data/

struct normalized stellar mass gradients, defined as $\bar{\Delta}M^*_{R_1R_2} = (M^*_{R_2} - M^*_{R_1})/M^*_{R_2}$, at specified radii ($R$=10, 19, 27, 36, 50, 69, 94, 130 kpc); this gives us 7 stellar mass gradients to work with. We also include ellipticity values at 13 radii (R=10, 12, 15, 18, 22, 26, 31, 37, 45, 54, 64, 77, 93 kpc), and ellipticity and position angle gradients at 11 radii (R=10, 15, 22, 26, 31, 37, 45, 54, 64, 77, 93, 111 kpc). Including the 2D axis ratio, then, we have a total of 43 features. For further exploration, we add mass (at two radii, R=10, 100 kpc, as well as the true total stellar mass) to check the dependency on the mass scale, as well as 4 second order parameters for "boxiness" and "asymmetry" at 7 radii (R=10, 12, 15, 18, 22, 26, 31, 37, 45, 54, 64, 77, 93, 111 kpc), adding 28 features.

2.3. *3D Shape*

2.4. *Axis Ratio Calculation*

Galaxies can most generally be modeled as ellipticals, with axes $a \geq b \geq c$. In order to calculate the axis ratios b/a, c/a for different galaxies, we adapt the code[3] presented in Li et al. (2018) to work with the simulated cutouts at $z = 0.4$ matching the HSC observations. With the axis ratios at hand, we move on to the task of shape classification; we discuss the choice of radius at which to evaluate the shape in Section 3.1.

2.5. *Shape Classification*

While 3D shapes might be defined broadly, e.g., prolates, oblates, triaxials, and sphericals, the classification has to be quantified precisely in order to use numerical methods to infer the 3D shape – a non-trivial tasks since classification criteria vary widely. For instance, Li et al. (2018) consider galaxies to be prolates if $b/a - c/a < 0.2, b/a < 0.8$, oblates if $b/a - c/a > 0.2, b/a > 0.8$, triaxials if $b/a - c/a > 0.2, b/a < 0.8$, while the rest are considered spherical.

On the other hand, Jiang et al. (2019) define the four classes using thresholds on flattening ($\equiv \sqrt{1-(c/b)^2}$) and elongation ($\equiv \sqrt{1-(b/a)^2}$): prolates are galaxies with flattening < 0.5 and elongation < 0.5, oblates with flattening ≥ 0.5 and elongation ≤ 0.5, triaxials with flattening ≥ 0.5 and elongation ≥ 0.5, while the rest are considered spherical.

For a simpler criteria, we consider a cut on the triaxiality parameter, defined as $T = \left(1-(b/a)^2\right) / \left(1-(c/a)^2\right)$. We define prolates as galaxies with $T > 0.7$ and the rest as not-prolates, motivated by e.g., Kimm & Yi 2007.

[3] https://github.com/HongyuLi2016/illustris-tools

2.6. *Machine Learning Algorithm*

As alluded to earlier, we make use of the Random Forests for our purposes, specifically since it allows us (an easy) access to feature importance that might indicate proxy features for the 3D shape. Specifically, we use the `RandomForestRegressor` available via `sci-kit`, with one-hot encoding to allow for 2+ way classification as well as regression. For simplicity however, we consider only a 2-way classification: prolates (`P`) vs. not-prolates (`Not-P`). We then optimize the hyperparameters using `RandomizedSearchCV` with 5-fold cross validation. Since we are working with imbalanced classes, we test the effectiveness of our classifier using the precision-recall curve, alongside the confusion matrices. Also, we re-run our classification with top-15 features selected from by the algorithm, allowing us to probe the validity of the importance of the features deemed important.

As for the data on which to train and test our algorithm, we consider Illustris and IllustrisTNG simulations separately since the underlying physical is somewhat different between the two; this allows us to probe the relation between 3D shape and 2D summary data in different spaces. For each, we use a 30-70% random split for test-train (although we find no strong dependence of our results on the split ratio).

3. RESULTS

3.1. *3D Shape Dependence on Radius*

In order to decide the radius based on which to classify galaxy shapes, we plot the profiles of change in the axis ratios and the triaxiality parameter; this is shown in Figure 2, with triaxiality-based shape classification. We see that while the axis ratios and the triaxiality parameter change for small radii, the changes are small for larger radii, indicating that the shape "settles" at the larger radii. Therefore, for our analysis from here on, we classify galaxies based on the shape parameters (axis ratios or triaxiality) at $R = 50$ kpc.

3.2. *3D Shape Classification Criteria: Comparisons*

In order to get an intuition into the classification methods, we plot the distribution of the axis ratios b/a, c/a as well as the the triaxiality parameter T for our galaxy samples. Figure 3 shows the distributions for the galaxies in our Illustris sample while Figure 4 shows the same for our IllustrisTNG galaxies. We see that not only do the three classification criteria lead to classifying different galaxies as different shapes, there is no intrinsic separation between the shape classes, at least not in the three distributions shown. We also note that overall distributions of the three parameters are similar between Illustris and IllustrisTNG samples.

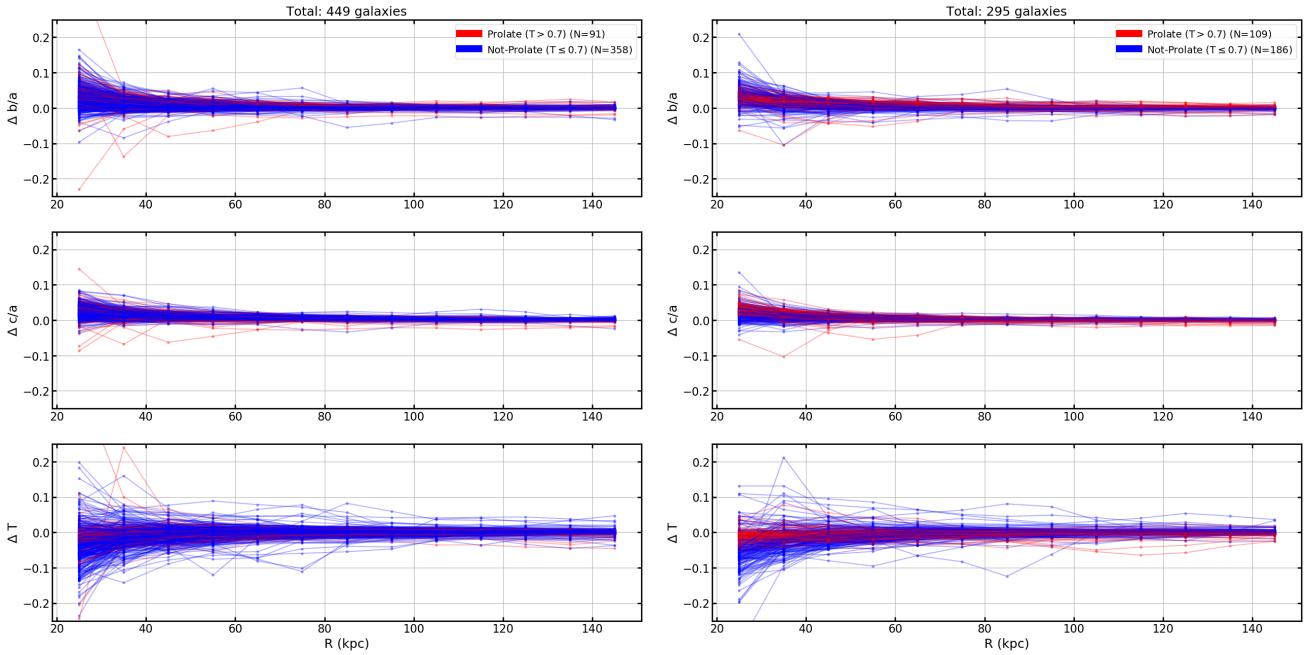

Figure 2. Difference in axis ratios and the triaxiality parameter as a function of radius for Illustris (left) and IllustrisTNG (right) samples, with triaxiality-based shapes. We note that all parameters settle at large ($R \gtrsim 50$ kpc) radii.

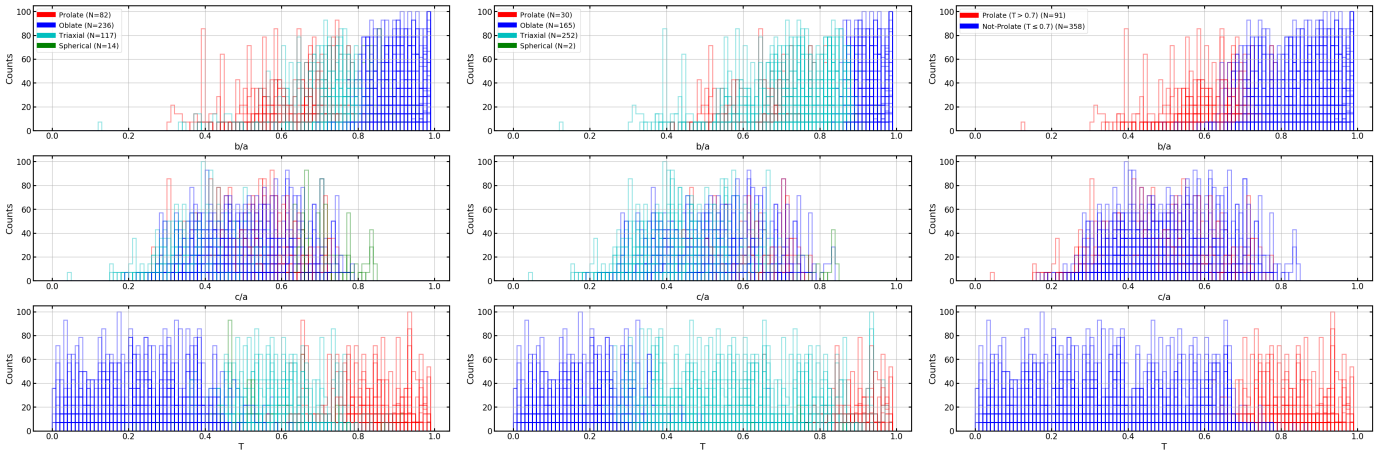

Figure 3. Distribution of axis ratios and the triaxiality parameter for Illustris galaxies, with shapes based on Li et al. (2018)'s criteria (left), Jiang et al. (2019)'s criteria (middle), and the triaxiality-based criteria (right). We see that there is no intrinsic separation between the three parameters for the various shape classes, and that the three classification criteria lead to rather different shape classifications.

We also compare the three classification criteria in the space of the two axis ratios. Figure 5 shows the axis ratios for the galaxies in our Illustris sample while Figure 6 shows them for IllustrisTNG. Comparing the panels within each figure, we see that while the three classification criteria largely show similar trends, they lead to different classifications. On the other hand, comparing the two figures, we see that the two simulations lead to similar trends except that IllustrisTNG leads to more prolates than Illustris.

As mentioned in Section 2.6, we proceed with just two classes: prolates (`P`) vs. not-prolate (`Not-P`), and consider only the Li et al. (2018)'s criteria and the triaxiality-based criteria. We check the number counts for `P` vs. `Not-P` galaxies in our train vs. test cases and find that Li et al. (2018)'s criteria leads to similar ratios for `P` vs. `Not-P` in Illustris and IllustrisTNG: for Illustris, we have a 93-7 split for training and 94-6 for test, while for IllustrisTNG, we have a 90-9 split for training and 92-8 for test. On the other hand, the triaxiality-based criteria leads to a 79-21 split for train-

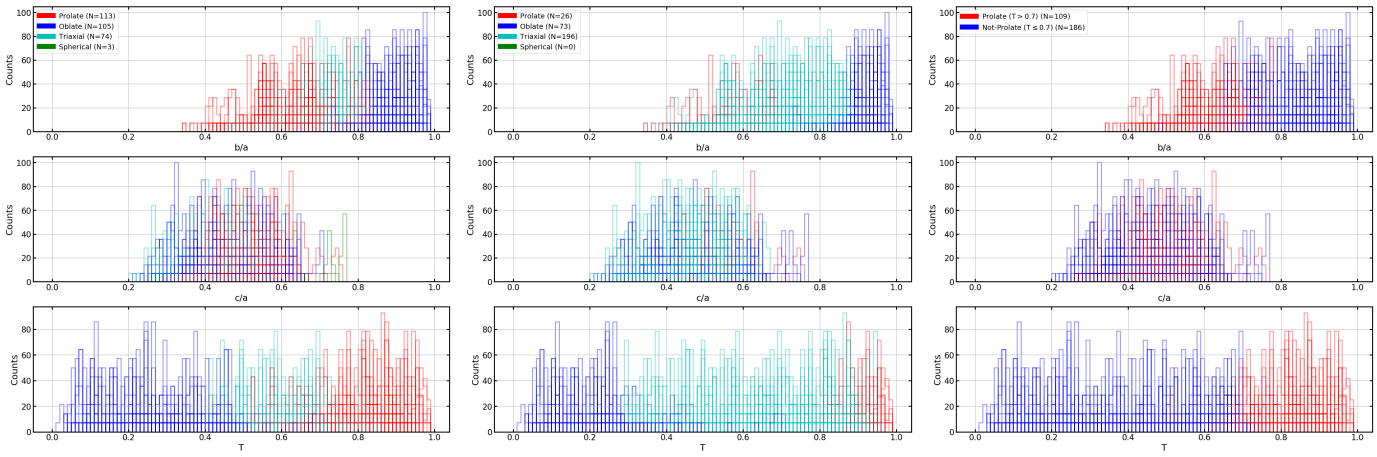

Figure 4. Distribution of axis ratios and the triaxiality parameter for IllustrisTNG galaxies, with shapes based on Li et al. (2018)'s criteria (left), Jiang et al. (2019)'s criteria (middle), and the triaxiality-based criteria (right). As in Figure 3, we see that there is no intrinsic separation between the three parameters for the various shape classes, and that the three classification criteria lead to rather different shape classifications.

ing and 81-17 split for test for the Illustris sample, and a 62-38 split for training and 66-34 split for test for the IllustrisTNG sample. These numbers are important since 1) they ensure that train and test sets are consistent for both simulations, and 2) they demonstrate that the two criteria lead to different degree of imbalance between the two classes.

3.3. *Prolate and Not-Prolate Fractions: Comparisons*

As a further check, and to gain understanding between the two simulations, we plot the prolate fraction for the Illustris and IllustrisTNG samples, especially to compare against Figure 3 in Li et al. (2018) which shows the apparent trend for Illustris galaxies at $z = 0$ that prolate fraction increases for higher stellar mass. Figure 7 shows the prolate fraction as a function of stellar mass alongside the number count of `P` galaxies vs. `Not-P` for Illustris and IllustrisTNG. We note a few important trends: we see a larger prolate fraction at higher masses for Illustris sample, in agreement with Li et al. (2018), while the same is not true for IllustrisTNG – a reassuring result since more prolates are expected at lower stellar mass in IllustrisTNG as major mergers are a dominant source of accretion in IllustrisTNG leading haloes to be more prolate (Tacchella et al. 2019). On the other hand, we note that the prolate fraction and its trends should be considered with caution given the low number count of galaxies, let alone that of prolates, at higher stellar masses. Nevertheless, we note the production of more prolates at lower stellar masses in IllustrisTNG as an importance divergence from Illustris; one that would especially have an impact on classification if overall mass is included as a feature in our training set. We compare the analog of Figure 7 from the other two classification criteria and find similar results.

3.4. *3D Shape and Summary Profiles*

To check the dependence of the mass and ellipticity on the 3D shape, we plot the profiles for galaxies at a fixed stellar masses (specifically those with $11.3 \leq \log_{10}(M^*_{\sim 30}/M_\odot) \leq 11.5$) for one of the three projections. These are shown in Figure 8 for Illustris galaxies and in Figure 9 for the IllustrisTNG galaxies. We see that while the mass profiles are comparable between the two simulations, we observe more prolate galaxies with higher ellipticity values in IllustrisTNG than in Illustris. These plots are instructive as they can be directly compared with observations.

3.5. *3D Shape Classification: Results*

Figure 10 shows the confusion matrices for the Illustris galaxies when training/testing with shape classification based on triaxiality. We see with `Not-P` (not-prolate) are classified more effectively while `P` (prolates) are not, while the results do not change significantly when we rerun our analysis with top-15 features, as selected by the Random Forest algorithm. Similarly, Figure 11 shows the analog figures for the IllustrisTNG galaxies, where we find that while `Not-P` galaxies are still classified more effectively than prolates, the discrepancy is not as strong for the Illustris sample. Also, similar to Illustris galaxies, the results do not change significantly when we rerun our analysis with top-15 features. Comparing Figures 10 and 11, however, we note the diverging trends between the two simulations, arising due to two possible reasons: 1) larger sample size available for Illustris leading to stronger results (better classification for

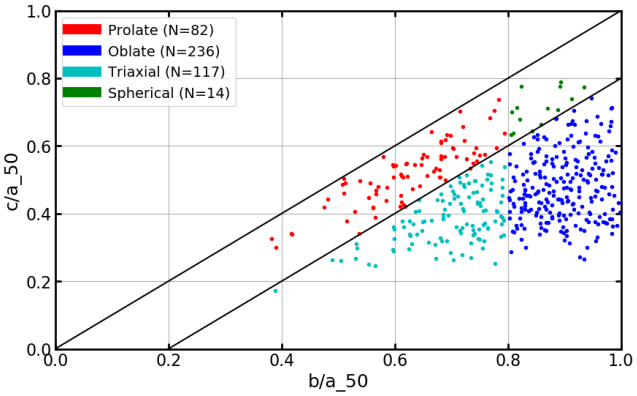

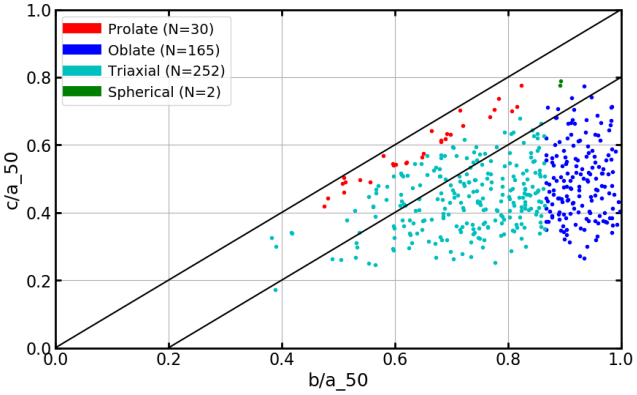

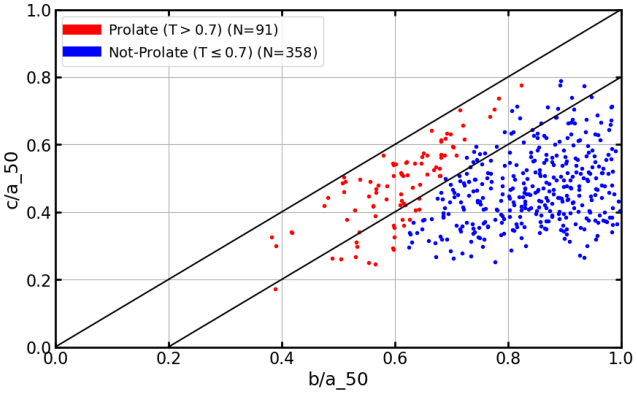

Figure 5. Axis ratios for Illustris galaxies, with shapes based on Li et al. (2018)'s criteria (top), Jiang et al. (2019)'s criteria (middle), and triaxiality (bottom). We see that the three criteria lead to different classification for the galaxies.

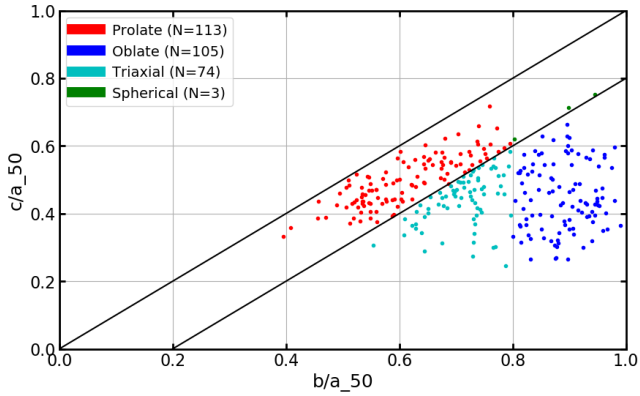

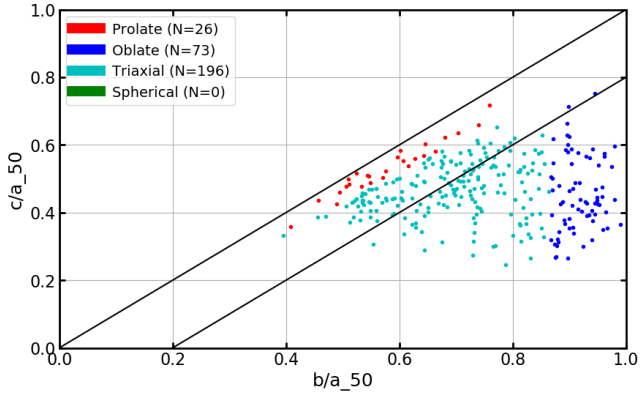

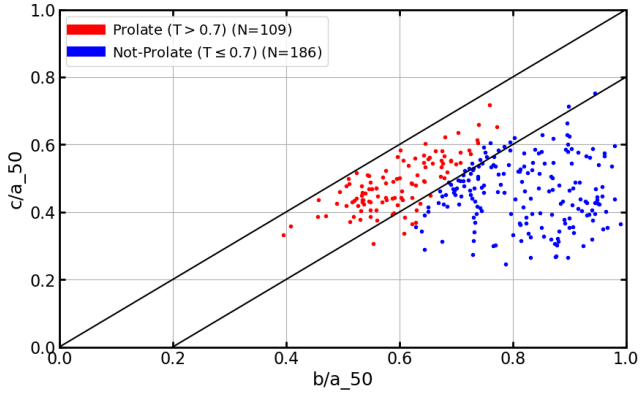

Figure 6. Axis ratios for IllustrisTNG galaxies, with shapes based on Li et al. (2018)'s criteria (top), Jiang et al. (2019)'s criteria (middle), and triaxiality (bottom). We see that the three criteria lead to different classification for the galaxies.

`Not-P` and more misclassification for `P`), and 2) the different underlying physics in the two simulations, leading to different characteristics of prolate galaxies.

As a more probing measure of the effectiveness of our classifier, we consider the precision-recall curve shown in Figures 12-13 for Illustris and IllustrisTNG galaxies respectively. Broadly, we note that our classifier does not perform significantly well (as it is far from the ideal of high precision, especially at high recall values), hinting at the strong degeneracy of the information available via the selected features. As before, we see that the performance is better for not-prolates than prolates, with Illustris sample leading to better results, and the results being consistent when considering all 43 features vs. top-15 ones. We note, however, that the optimization of the algorithm leads to the jaggedness of the curve, without delivering significant gain in the overall precision-recall trend.

If we include mass as a feature, we find that the precision-recall results improve modestly for both Illustris and IllustrisTNG galaxies. Similarly, adding the

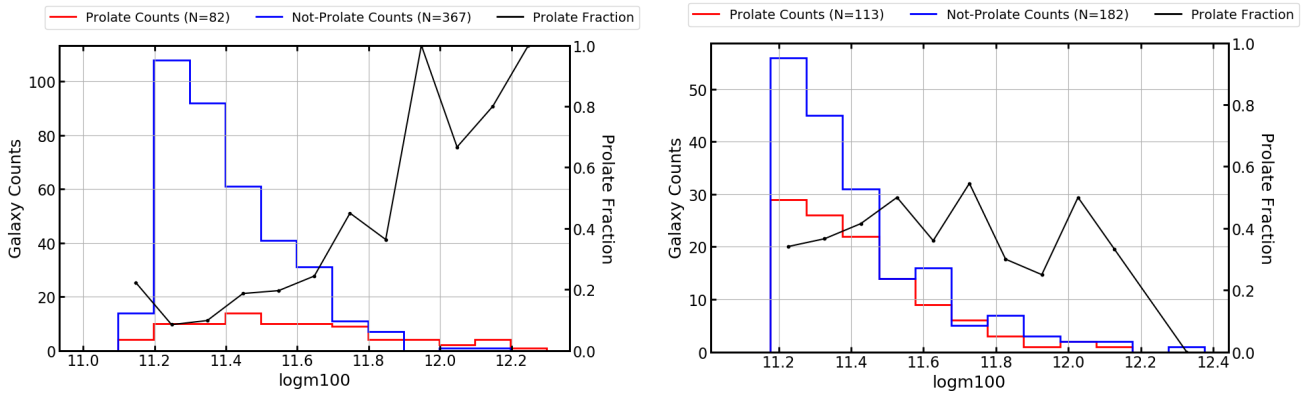

Figure 7. Prolate fraction and galaxy counts as a function of stellar mass for Illustris (left) and IllustrisTNG (right) galaxies, with shapes based on Li et al. (2018)'s criteria. Comparing these with Figure 3 in Li et al. (2018), we see that while we recover the trend of larger prolate fraction for higher stellar mass for the Illustris sample, the number counts are not high enough to rule out effects of Poisson noise. Also, we do not see the trend for the IllustrisTNG sample, illustrating a difference in the underlying physics between the two simulations.

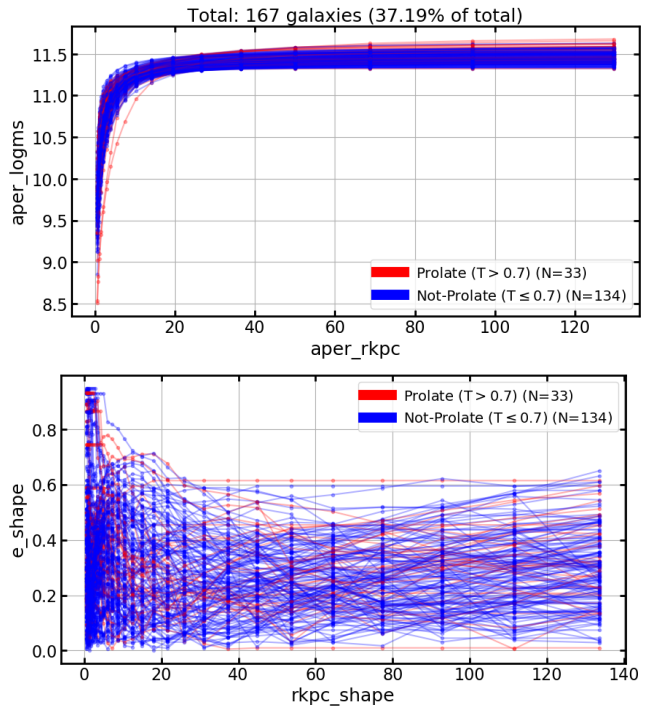

Figure 8. Mass (top) and ellipticity (bottom) profiles for one of the three projections for Illustris galaxies with $11.3 \leq \log_{10}(M^*_{\sim 30}/M_\odot) \leq 11.5$, with shapes based on the triaxiality-based criteria.

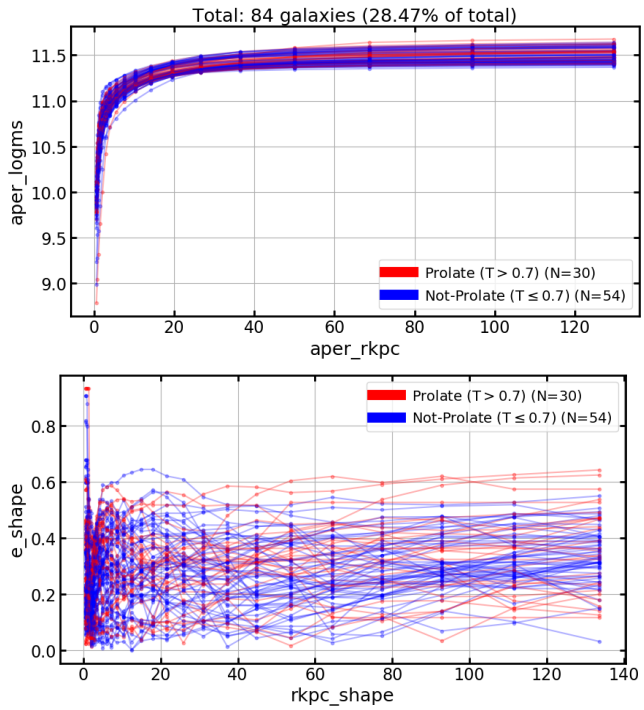

Figure 9. Mass (top) and ellipticity (bottom) profiles for one of the three projections for IllustrisTNG galaxies with $11.3 \leq \log_{10}(M^*_{\sim 30}/M_\odot) \leq 11.5$, with shapes based on the triaxiality-based criteria.

second order parameters, described in Section 2.1, helps similarly for both Illustris and IllustrisTNG galaxies.

As for results for shapes using Jiang et al. (2019)'s criteria, our model performs well for not-prolates but terribly for prolates. We are investigating the reasons to explain the trends.

3.6. *Important Features for 3D Shape*

As mentioned before, one of our goals is to identify 2D features that may be strong proxies for the 3D shape. Our choice of machine learning algorithm helps with identifying these features as the Random Forest algorithm produces feature importance - a metric encapsulating how helpful a given input feature is for identifying the target. Using the output features importance,

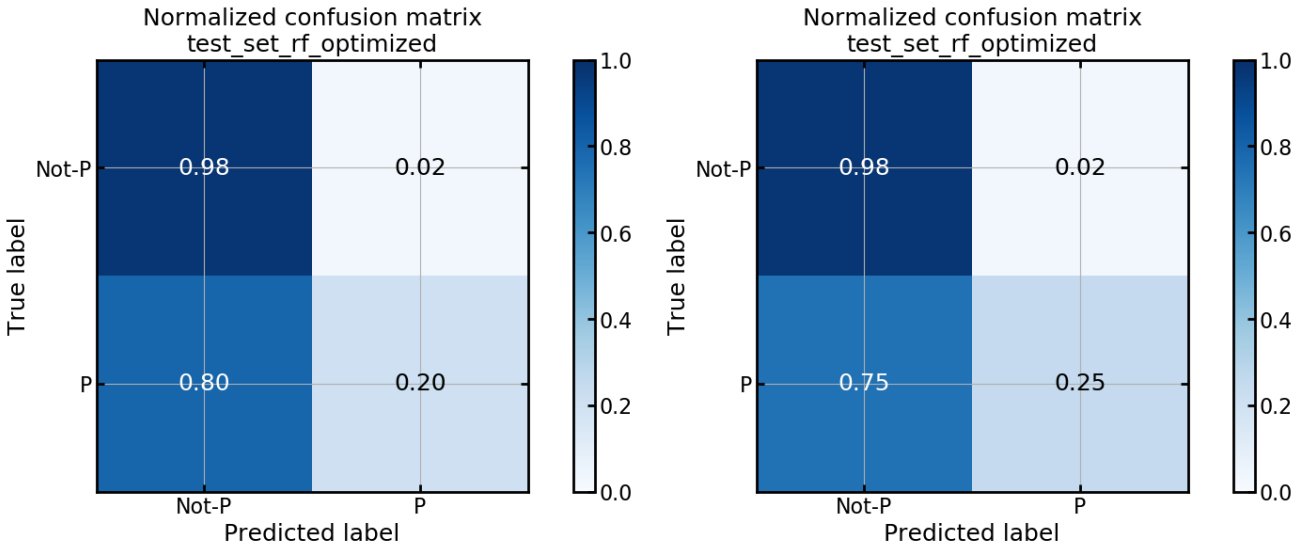

Figure 10. Confusion matrices for Illustris galaxies with triaxiality-based shapes, when trained with all 43 features (left) and when trained with top-15 only (right). We see that our classifier is more effective for `Not-P` galaxies than for `P` ones, while the results are robust to features that are deemed important by the classifier.

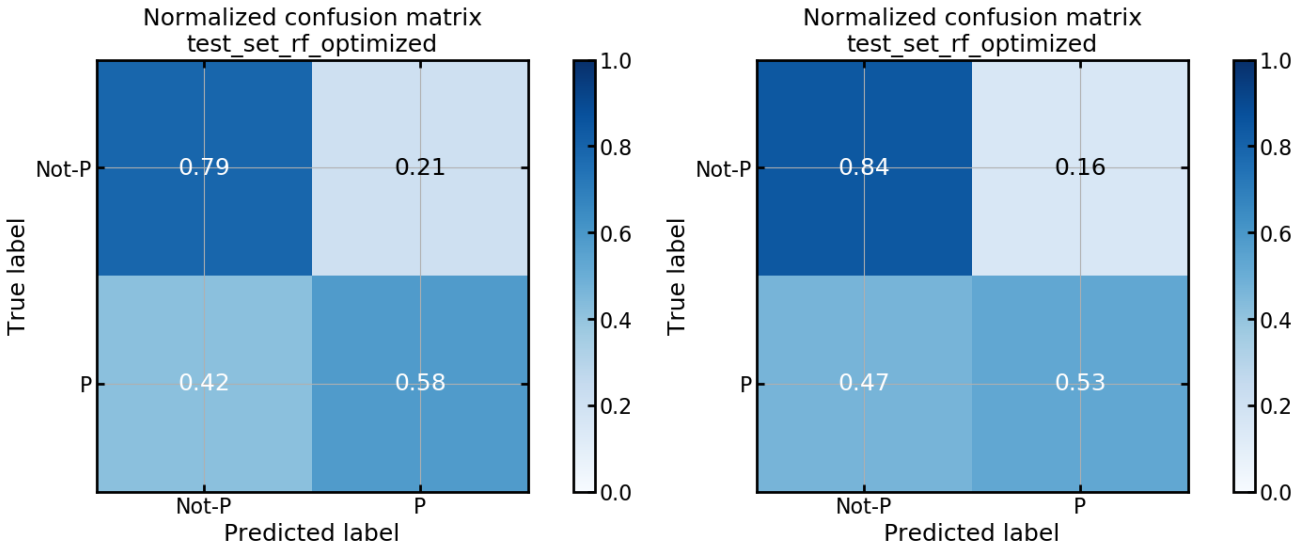

Figure 11. Confusion matrices for IllustrisTNG galaxies with triaxiality-based shapes, when trained with all 43 features (left) and when trained with top-15 only (right). We see that our classifier is more effective for `Not-P` galaxies than for `P` ones, while the results are robust to features that are deemed important by the classifier.

we find that the normalized mass gradients have strong impacts, although, as can be inferred from some of the results discussed in Section 3.5, no feature is incredibly important: while the importance can range form 0-1, the maximum importance we see is 0.1. Nevertheless, it is instructive to consider the features that are ranked higher than the others. For Illustris, the top five features are normalized mass gradients for $(R_{\rm in}, R_{\rm out}) = (94, 130), (69, 94), (19, 27), (50, 69), (10, 19)$ kpc in the order of decreasing importance, while for IllustrisTNG galaxies, the top five features are four normalized mass gradients for $(R_{\rm in}, R_{\rm out}) = (10, 19), (69, 94), (94, 130), (36, 50)$ kpc and the ellipticity gradient at $(R_{\rm in}, R_{\rm out}) = (31, 37)$ kpc.

As an example, Figure 14 shows the distribution of the normalized mass gradient at $(R_{\rm in}, R_{\rm out}) = (69, 94)$ kpc since it is ranked important for both galaxy samples. We see that while the underlying distribution of the prolate vs. not-prolates galaxies for the features is different, distinguishing them completely is rather challenging.

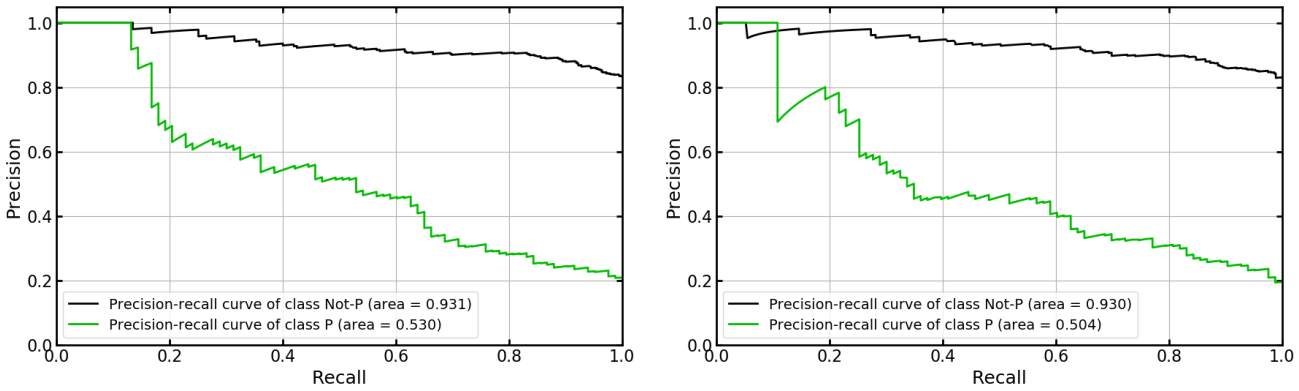

Figure 12. Precision-recall curves for Illustris galaxies with triaxiality-based shapes, when trained with all 43 features (left) and when trained with top-15 only (right). We see that while our classifier is not optimal, it is more effective for `Not-P` galaxies than for `P` ones; the results are robust to features that are deemed important by the classifier.

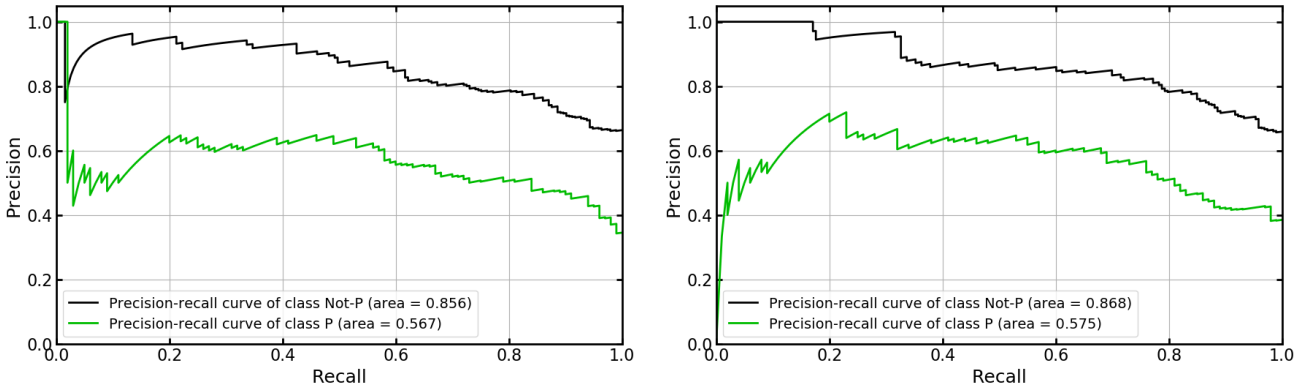

Figure 13. Precision-recall curves for IllustrisTNG galaxies with triaxiality-based shapes, when trained with all 43 features (left) and when trained with top-15 only (right). We see that while our classifier is not optimal, it is more effective for `Not-P` galaxies than for `P` ones; the results are robust to features that are deemed important by the classifier.

4. DISCUSSION AND CONCLUSIONS

In this work, we have attempted to use machine learning for 3D shape classification of galaxies. For this purpose, we have used the simulated galaxies from Illustris and IllustrisTNG for training/testing with Random Forest machine learning algorithm. We find that while our classifier is not optimal, it is able to learn important information from summary statistics of the 2D projections of the 3D galaxies, and is able classify galaxies correctly to a limited extent, alongside identifying features that may be strong proxies for the 3D galaxy shape.

There are various avenues for optimizing our supervised learning model to achieve better results. These include characterising the various features in a better way, e.g., instead of using arbitrary radii to sample the profiles of various statistics (e.g., mass, ellipticity, etc.), we could characterize them more effectively by considering the slope and intercept of the profiles in coarse, well-defined bins that are the same across the various statistics. Furthermore, we can include isophotal twisting and the concentration as features, as they are measurable quantities that may provide important information, alongside considering other proxies for the 3D shape (e.g., Shankar & Khatri 2019). Optimizing the features may allow us to optimize our algorithm to classify 3D galaxy shape effectively. Note that even if our algorithm is unable to classify shapes perfectly, identifying important features is very much an achievable deliverable.

Furthermore, we can extend our method to include the merger history as a feature, and probe the relation between mergers and 3D shape seen in the simulations (Li et al. 2018), i.e., galaxies with more mergers tend to be prolate. Another avenue for development is to check if our results can provide priors for the Bayesian inference to infer 3D shapes of observed galaxies.

ACKNOWLEDGEMENTS

We thank Carlo Cannarozzo, Nesar Ramachandra, Ivana Damjanov, Marc Hueras-Company, and Fangzhou Jiang for helpful convervations, alongside other participants of the 2019 Kavli Summer Program in Astrophysics. This work was initiated during the Kavli Sum-

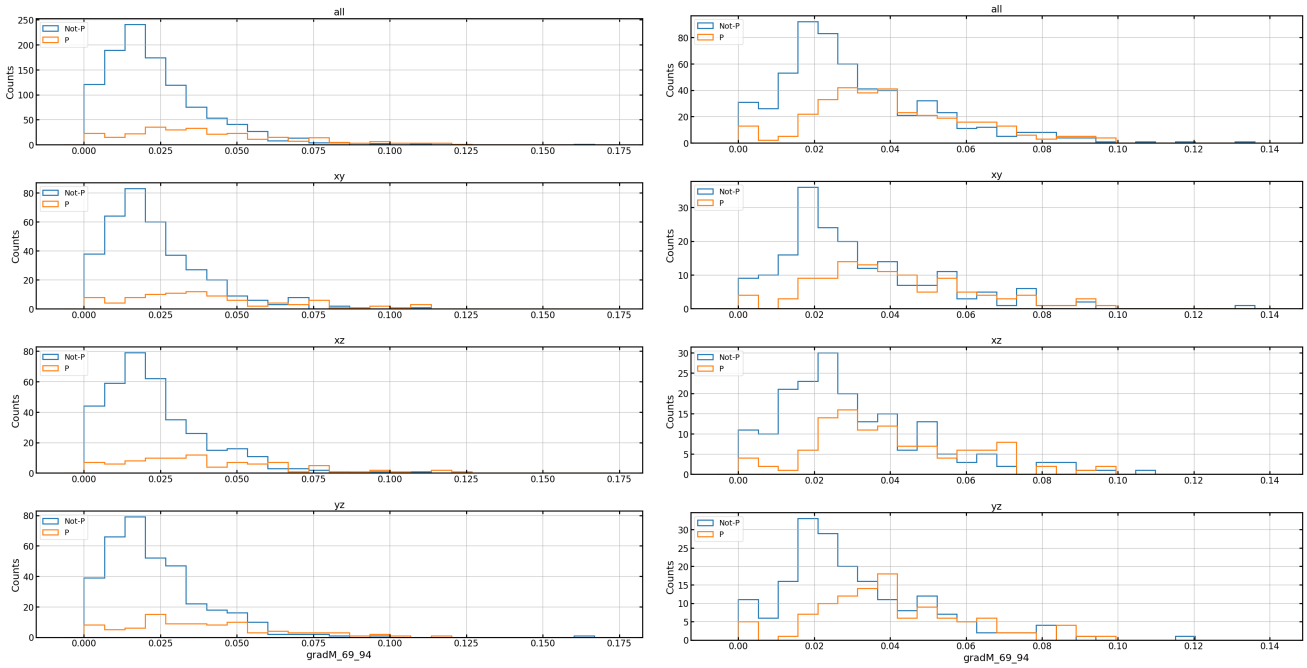

Figure 14. Distribution of normalized mass gradient at $(R_{\rm in}, R_{\rm out}) = (69, 94)$ kpc for Illustris (left) and IllustrisTNG (right) for all three projections (top row) and each of the three independent projections (row 2-4). Note that the galaxies are classified based on the triaxiality-based classification criteria.

mer Program in Astrophysics, funded by the Kavli Foundation, the National Science Foundation, and UC Santa Cruz. We thank the program for their support. HA has been supported by the Department of Energy (grant DE-SC0010008), and the Rutgers University & Bevier Dissertation Completion Fellowship.

REFERENCES

Ceverino, D., Primack, J., & Dekel, A. 2015, Monthly Notices of the Royal Astronomical Society, 453, 408

Huang, S., Leauthaud, A., Greene, J. E., et al. 2018, MNRAS, 475, 3348

Jiang, F., Dekel, A., Freundlich, J., et al. 2019, MNRAS, 487, 5272

Kimm, T., & Yi, S. K. 2007, The Astrophysical Journal, 670, 1048

Kormendy, J., Fisher, D. B., Cornell, M. E., & Bender, R. 2009, ApJS, 182, 216

Li, H., Mao, S., Emsellem, E., et al. 2018, MNRAS, 473, 1489

Naiman, J. P., Pillepich, A., Springel, V., et al. 2018, MNRAS, 477, 1206

Nelson, D., Pillepich, A., Springel, V., et al. 2018, MNRAS, 475, 624

Pillepich, A., Nelson, D., Hernquist, L., et al. 2018a, MNRAS, 475, 648

Pillepich, A., Springel, V., Nelson, D., et al. 2018b, MNRAS, 473, 4077

Shankar, S., & Khatri, R. 2019, arXiv e-prints, arXiv:1908.04454

Springel, V., Pakmor, R., Pillepich, A., et al. 2018, MNRAS, 475, 676

Tacchella, S., Diemer, B., Hernquist, L., et al. 2019, MNRAS, 487, 5416

Vogelsberger, M., Genel, S., Springel, V., et al. 2014, MNRAS, 444, 1518